Zn/Sr dual ions-collagen co-assembly hydroxyapatite enhances bone regeneration through procedural osteo-immunomodulation and osteogenesis

Zhenyu Zhong [a,b,1], Xiaodan Wu [a,b,1], Yifan Wang [a,b], Mengdie Li [a,b], Yan Li [a,b], XuLong Liu [a,b], Xin Zhang [a,b], Ziyang Lan [d], Jianglin Wang [a,b,c], Yingying Du [a,b,c,*], Shengmin Zhang [a,b,c,**]

[a] Advanced Biomaterials and Tissue Engineering Center, Huazhong University of Science and Technology, Wuhan, 430074, China
[b] Department of Biomedical Engineering, Huazhong University of Science and Technology, Wuhan, 430074, China
[c] Institute of Regulatory Science for Medical Devices, Huazhong University of Science and Technology, Wuhan, 430074, China
[d] Department of Biomedical Engineering, The University of Texas at Austin, Austin, TX, 78712, USA

ABSTRACT

The immune microenvironment induced by biomaterials played vital roles in bone regeneration. Hydroxyapatite (HA) and its ion-substituted derivates represent a large class of core inorganic materials for bone tissue engineering. Although ion substitution was proved to be a potent way to grant HA more biological functions, few studies focused on the immunomodulatory properties of ion-doped HA. Herein, to explore the potential osteoimmunomodulatory effects of ion-doped HA, zinc and strontium co-assembled into HA through a collagen template biomimetic way (ZnSr-Col-HA) was successfully achieved. It was found that ZnSr-Col-HA could induce a favorable osteo-immune microenvironment by stimulating macrophages. Furthermore, ZnSr-Col-HA demonstrated a procedural promoting effect on osteogenic differentiation of bone marrow mesenchymal stem cells (BMSCs) in vitro. Specifically, the osteo-immune microenvironment acted as a dominant factor in promoting osteogenic gene expressions at the early stage through OSM signal pathway. Whereas the direct stimulating effects on BMSCs by Zn^{2+}/Sr^{2+} were more effectively at the later stage with Nfatc1/Maf and Wnt signals activated. In vivo study confirmed strong promoting effects of ZnSr-Col-HA on critical-sized cranial defect repair. The current study indicated that such a combined biomaterial design philosophy of dual ion-doping and biomimetic molecular co-assembly to endow HA applicable osteoimmunomodulatory characteristics might bring up a new cutting-edge concept for bone regeneration study.

1. Introduction

Immune and skeletal systems are closely related because they share a number of cytokines, receptors, signaling molecules, and transcription factors. In addition, immune cells also play critical roles in bone homeostasis [1,2]. Thus, when bone implant materials are used in therapeutics, the body's immune response to them is an important factor to consider. Being an essential part of host immune response, immune cells have been studied extensively, especially macrophages, which play a central role in the early period of inflammation and host defense in

trauma repair [3]. Traditional osteoimmunology showed that M2 macrophage was more closely associated with osteogenesis, and biomaterials that induced M2 polarization promoted bone formation [4,5]. Whereas, some recent studies found that inflammatory macrophage (M1) could also induce osteogenesis in marrow mesenchymal stem cells (MSCs) via Oncostatin M (OSM) pathway [6]. Although there is no consensus on which macrophage phenotype is most beneficial for osteogenesis, it is beyond doubt that an appropriate immune environment at a specific time induced by implanted biomaterials was crucial for bone regeneration. As a result, the immunomodulatory effects of

bone implants have drawn widespread attention when devising advanced biomaterials.

Hydroxyapatite (HA), a widely used orthopedic material, has many advantages such as biocompatibility, osteoconductivity, and osteoinductivity [7–9]. To achieve enhanced bone regeneration, many factors still need to be taken into account when a hydroxyapatite-based biomaterial is designed, including particle size [10], morphology [11], and crystallinity [12]. Various methods have emerged to improve the hydroxyapatite-based materials' biological performance, such as element doping, heat treatment, material cladding, etc. [13–15]. Among these, inorganic ion doping is an important strategy for modifying hydroxyapatite-based materials because the substituted ions have a crucial influence on the structure, composition, and mechanical properties of the mineral phase. Many inorganic ions, such as zinc (Zn), strontium (Sr), copper (Cu), magnesium (Mg), manganese (Mn), and silicon (Si), have been successfully doped into hydroxyapatite with enhanced bone repair outcomes [16–21]. The co-doping of multi-ions further endows hydroxyapatite with more versatility [22–24]. However, inconsistent results between *in vitro* and *in vivo* studies suggested that more attention should be paid to the host immune response after biomaterial implantation [25]. So far, few studies focused on the effects of ion-doped hydroxyapatite on immune systems. Thus, the related osteoimmunomodulatory capability should be seriously considered when designing and evaluating ion-doped hydroxyapatite.

Ion-doped hydroxyapatite can generally be synthesized through wet or dry chemistry methods in different ways, including precipitation, hydrothermal, and sol–gel methods [26]. Among them, the method of organic template-mediated biomimetic molecular self-assembly tends to be more suitable than others for ion doping of hydroxyapatite [27], because the products were highly biocompatible and structurally similar to bone minerals. Especially when type I collagen, the main organic component of bone, was used as a template, the ion-substituted hydroxyapatite exhibited outstanding ability in promoting bone formation [28,29]. Therefore, in this study, we proposed to co-assemble

ion-substituted hydroxyapatite with collagen template in a biomimetic way, aiming to explore the potential osteoimmunomodulatory effects of ion-substituted hydroxyapatite and blaze a trail for designing and evaluating advanced hydroxyapatite-based biomaterials. Previous studies have shown that Zn and Sr, two vital trace elements in bone, play vital roles in immunomodulation, bone development, and bone reconstruction [30–32]. Thereby, Zn and Sr were chosen here to co-assemble ion-substituted hydroxyapatite with collagen as the organic template (ZnSr-Col-HA). Then, the osteoimmunomodulatory effect of ZnSr-Col-HA *in vitro* was assessed by monitoring the macrophage behaviors. The osteogenic potential of ZnSr-Col-HA was further studied by exploring the effects of the immune microenvironment induced by ion-doped hydroxyapatites on the behaviors of rat bone marrow stromal cells (BMSCs). Finally, the *in vivo* rat critical-size cranial defect model was utilized to further investigate the osteogenic capacity of ZnSr-Col-HA (Fig. 1).

2. Materials and methods

2.1. Synthesis and characterization of ion-doped biomimetic co-assembled hydroxyapatite

Unless specifically stated, all the reagents used here were bought from Sinopharm group chemical reagent co. LTD and under reagent grade. Type I collagen was extracted from the rat tail with a modified method [33]. Briefly, the rat tail tendon was carefully separated with a tweezer, then rinsed with PBS to remove visible contaminants. 0.2 M acetic acid containing 1 wt% pepsin was prepared to dissolve the rat tail tendon at 4 °C overnight [v (acetic acid): m (rat tail tendon) = 30:1]. The viscous fluid product was precipitated with 2 M sodium chloride solution, and the supernatant was discarded after centrifugation. Repeat the former steps twice to get purified collagen products. The collagen was then dissolved with 0.2 M acetic acid, dialyzed in deionized water for 3 days. Finally, the obtained gel was frozen at −20 °C for 12 h and
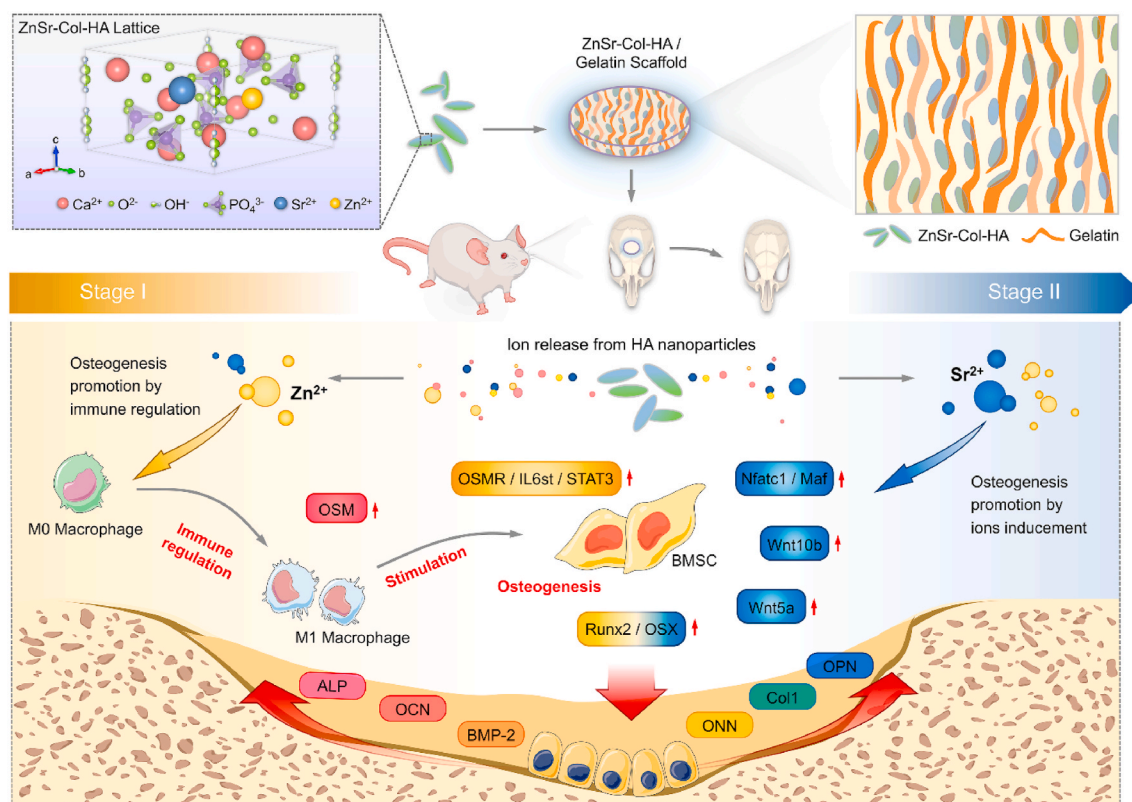
Fig. 1. Schematic diagram of ZnSr-Col-HA promoting bone regeneration through procedural osteo-immunomodulation and osteogenesis.

lyophilized for 2 days. The product collagen was stored at −20 °C for further use.

Ion-doped hydroxyapatite was co-assembled with the collagen template through a biomimetic way [34]. The basic formula for the material dictates that the molar ratio of Ca/P or (Ca + Zn + Sr)/P in the theoretical product is 1.67:1, and the collagen weight accounts for 30% of the total weight. Therefore, 2.36 g Ca(NO$_3$)$_2$·4H$_2$O and 0.43 g collagen were added to 100 mL deionized water, then the pH of the mixture was adjusted to 3.0 with 1 M HNO$_3$ to facilitate the collagen dissolution with mechanical stirring. After adding 2.15 g Na$_2$HPO$_4$·12H$_2$O, the mixture pH was adjusted to 8.0 with 1 M NaOH. The mixture was mechanically stirred at 350 rpm and kept at 37 °C for 24 h to continue the reaction. The precipitated product was collected by centrifugation at 8000 rpm for 10 min and rinsed with deionized water, after which they were freeze-dried and, the obtained powders were labeled as Col-HA. The Zn/Sr individually or co-substituted hydroxyapatite, noted as Zn-Col-HA, Sr-Col-HA, and ZnSr-Col-HA, respectively, were synthesized through a similar process. The calcium component was partly replaced by 5 mol% Zn(NO$_3$)$_2$·6H$_2$O, 5 mol% Sr(NO$_3$)$_2$, and 5 mol% Zn (NO$_3$)$_2$·6H$_2$O plus 5 mol% Sr(NO$_3$)$_2$. All hydroxyapatite samples were ground carefully with an agate mortar for further use.

The morphology and structure of hydroxyapatite were observed by scanning electron microscopy (SEM, Nova NanoSEM 450, FEI, Holland) and transmission electron microscopy (TEM, Tecnai G2 F30, FEI, Holland). High-resolution TEM images were also acquired by Tecnai G2 F30. The molar ratio of (Ca + Zn + Sr)/P was measured by X-ray fluorescence (XRF, EAGLE III, EDAX, USA) spectroscopy. The crystalline phase data were recorded on an X-ray diffractometer (XRD, Shimadzu, Kyoto, Japan) with Cu-Kα radiation and compared with the standard data (PDF No. 09–0432). The functional groups were identified by Fourier transform infrared spectroscopy (FTIR; VERTEX 70, Bruker, Germany). The Zn/Sr release profile of ion-doped hydroxyapatite in Dulbecco's modified eagle medium (DMEM) was measured by atomic absorption spectrum (AAS, SPM9700, Shimadzu, Japan). Briefly, 0.1 g hydroxyapatite powder was immersed in 4 mL DMEM, 3 mL supernatant was collected by centrifugation at appointed time points, and another 3 mL fresh DMEM was supplemented to the original suspension for sequential ion release. The Zn/Sr ion concentration in the supernatant was detected by AAS at each time point. Thermogravimetry (TGA) and differential scanning calorimetry (DSC) analysis were carried out with STA449F3.

2.2. Cell culture

In this study, the murine-derived macrophage cell line RAW264.7 (RAW) and rat bone marrow stromal cells (BMSCs) were purchased from iCell Bioscience Inc, Shanghai. Both cells were cultured and expanded in Dulbecco's Modified Eagle Medium (DMEM, Gibco, Invitrogen, USA) supplemented with 10% fetal bovine serum (FBS, Gibco, Product number 16170078) and 1% penicillin/streptomycin (P/S, Gibco, Product number 15140122) in a 5%CO$_2$-incubator at 37 °C. Both cells were passaged when the cell confluence rate was over 80%. Passages 3–5 of BMSCs were used in the following experiments. Mouse primary macrophage cell (Cat NO.: CP-M141) was purchased from Procell Life Science & Technology Co., Ltd, Wuhan.

2.3. Viability of macrophages and BMSCs cultured with the extraction of hydroxyapatite materials

Four hydroxyapatite materials, Col-HA, Zn-Col-HA, Sr-Col-HA, and ZnSr-Col-HA, were leached with DMEM at a concentration of 25 mg/mL in a 37 °C 5%CO$_2$-incubator for 24 h separately. The resulting extraction was sterilized with 0.2 µm filter membranes and stored at 4 °C for further use. To evaluate the materials' cytocompatibility, RAW and BMSCs were cultured with the former extraction supplemented with 10% FBS and 1% P/S for 1/3/7 days. In addition, 24-well transwell

(Guangzhou Jet Bio-Filtration Co., Ltd, TCS005024) were used for co-culturing experiment of RAW and BMSCs. RAW and BMSCs were seeded in upper chamber and bottom well of transwell respectively. At each time point, the cell viability of BMSCs was evaluated by cell counting kit-8 (CCK-8, Beyotime Biotechnology, C0038).

2.4. The osteo-immune response of macrophages cultured in material extraction

Macrophages (RAW and mouse primary macrophage cells) were seeded at the density of 1.5×10^5 cells/well in 6-well plates. After a 24-h culture process, the medium was replaced with the four aforementioned extractions (supplemented with 10% FBS, 1% P/S), followed by another 24-h culture. The supernatant was centrifuged at 3000 rpm for 10 min, then supplemented with dexamethasone, ascorbic acid, and β-glycerophosphate to a final concentration of 0.1 nM, 50 mM, and 10 mM, respectively, and labeled as the conditioned medium, stored at 4 °C for further use. The ion concentrations of different supernatants were determined by Inductively Coupled Plasma Optical Emission Spectrometer (ICP-OES). mRNA was isolated from the cells with a Total RNA Kit (HP Total RNA Kit, OMEGA, R6812-02). 2.5 µg RNA was used to synthesize complementary DNA (cDNA) using the Hifair ®III 1st strand cDNA Synthesis SuperMix (Yeasen Biotech Co., Ltd., 11141ES60) following the instructions. mRNA expression of inflammatory cytokines and osteogenic factors from RAW was quantified by RT-qPCR on ABI Prism 7500 Thermal Cycler (Applied Biosystems, Foster City, California, USA) using SYBR Green qPCR Master Mix (Vazyme Biotech Co., Ltd, Q711-02). RT-qPCR primers applied here were listed in Table S1. The ΔΔCt method was applied for evaluating the gene expression level, compared with housekeeping gene 18 s.

In the flow cytometry experiment, RAW cells and mouse primary macrophages were seeded in 12-well plate with the density of 3×10^4 cells/cm^2. After 24 h of incubation, the complete medium was replaced with four kinds of conditioned medium above-mentioned. After another 24 h of culturing, the cells were digested and collected in 1.5 ml epoxy resin tube, washed twice using PBS. Then cells were labeled with CD86 antibody (Biolegend, 105001). After reaction in the dark at room temperature for 20 min, cell samples were analyzed by Flow Cytometer (CytoFLEX, BECKMAN, USA).

2.5. The osteogenic differentiation of BMSCs under the stimulation of conditioned media

To evaluate the osteoimmunomodulatory effects of different hydroxyapatite materials on BMSCs, the BMSCs were cultured with the conditioned medium, and the expression levels of osteogenic factors and proteins were measured. For osteogenic gene expression analysis by RT-qPCR, BMSCs were cultured in 6-well plates at the density of 1.5×10^5 cells/well for 24 h using the complete medium. After replacing by the conditioned medium, BMSCs were cultured for another 3/7 days. Total RNA was collected, and osteogenesis-related gene expression levels were analyzed by RT-qPCR as described above. RT-qPCR primers applied here were listed in Table S2, β-actin was chosen as a housekeeping gene.

As a key osteogenic marker of osteoblastic differentiation, alkaline phosphatase (ALP) expression was stained by BCIP/NBT and quantified by LabAssay™ ALP kit (Wako, Japan) according to the manufacturer instructions. Images were captured by a light microscope after dyeing was finished. BMSCs used for ALP staining and quantification were seeded in 24-well plates at a density of 5×10^4 cells/well.

2.6. The in vivo evaluation on osteogenic effect and immune microenvironment of ion-doped hydroxyapatite

After a series of *in vitro* studies, we applied a subcutaneous implantation model to evaluate effect of ion-doped hydroxyapatite on immune microenvironment as reported previously [35]. The critical-sized

Sprague-Dawley (SD) rat cranial defect model was also used to evaluate the material's promoting effects on bone regeneration *in vivo*. The composite scaffolds used in the animal experiment were prepared by mixing the designated hydroxyapatite powder (Col-HA, Zn-Col-HA, Sr-Col-HA, and ZnSr-Col-HA) with gelatin solution (15 w/v%). The mass ratio of HA to gelatin was predetermined as 7:3, mimicking the natural bone composition. After well mixing with vortex, the slurry was transferred to a silicone rubber mold with cylindrical cavities (8 mm as diameter, 2 mm as height), quenched by liquid nitrogen, and lyophilized

for 2 days. The resulting scaffolds were crosslinked with 2.5% glutaraldehyde solution for 5 min, then rinsed with 1 wt% glycine solution three times to completely remove the residual glutaraldehyde. After completely removing the moisture by lyophilizing, the scaffolds were sterilized with 10 kGy cobalt-60 radiation before use.

All animal procedures were approved by the Institutional Animal Care and Use Committee at Huazhong University of Science and Technology (HUST). The male SD rats involved in this study were 200–220 g. Each rat was anesthetized with isoflurane during surgery. Dorsal regions
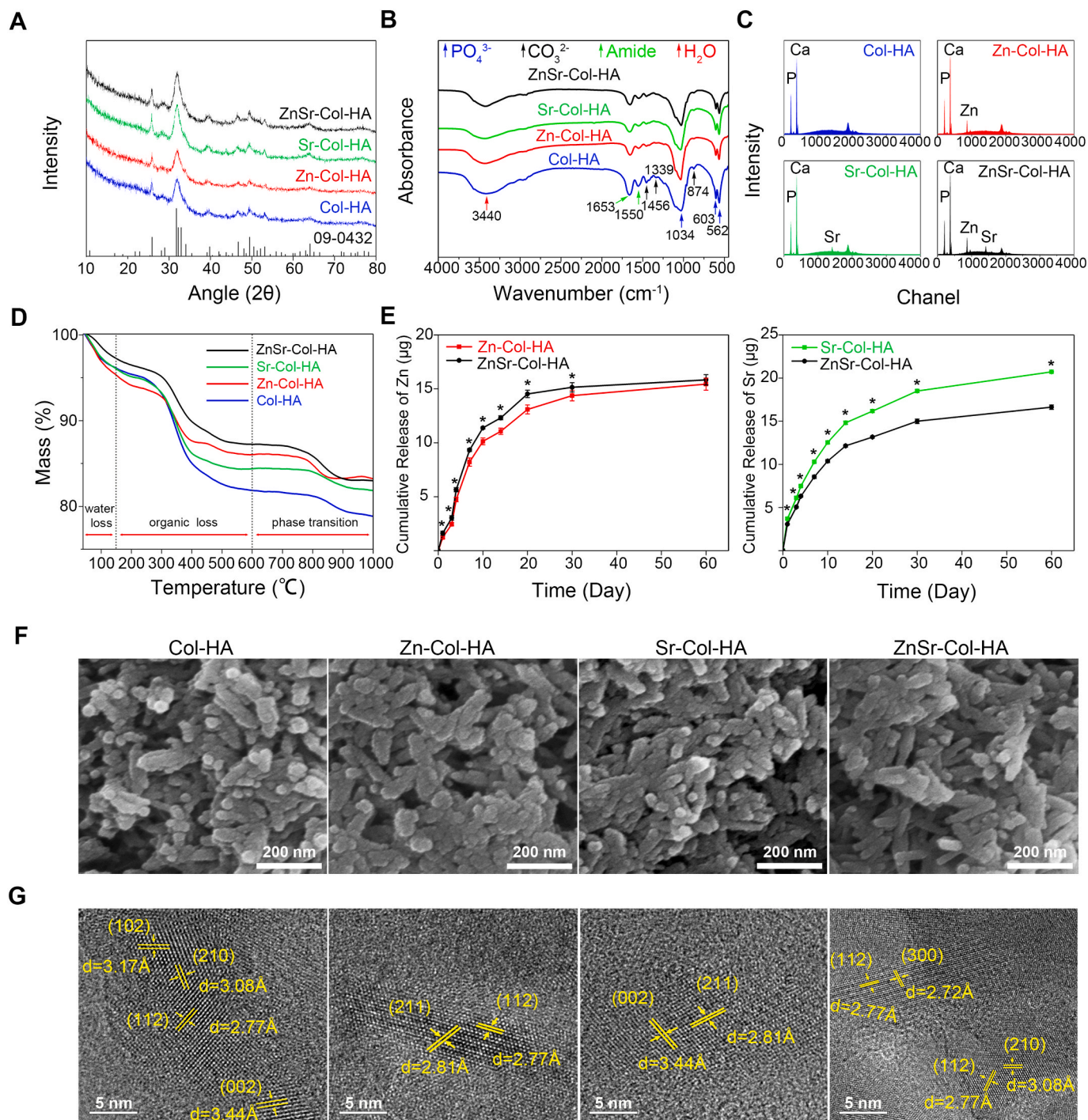
Fig. 2. Characterization of ion-doped hydroxyapatites. (A) XRD analysis and (B) FTIR spectrums showed the typical characteristic peaks of hydroxyapatite. (C) XRF results proved that Zn/Sr individually and jointly incorporated into hydroxyapatite successfully. (D) TGA results of different hydroxyapatites. (E) Zn and Sr cumulative release curves showed continuous-release characteristics in all ion-doped hydroxyapatite. *$p < 0.05$, indicated that there was a significant difference of released ions content between the two groups. (F) SEM, (G) HR-TEM images of Col-HA, Zn-Col-HA, Sr-Col-HA, and ZnSr-Col-HA, respectively.

of each rat were shaved and disinfected, and four sagittal incisions on the skin were created. Then, the four kinds of scaffolds were implanted, and the surgical cut was closed by suturing. After 3 days animals were sacrificed. Scaffolds and whole layer of skin around surgical sites were together harvested. The harvested samples were fixed in 4% para-formaldehyde and embedded in paraffin. Then the samples were cut into 5 μm thick sections for hematoxylin-eosin (H&E) staining and immu-nofluorescence (IF) assay of CD86. As for the SD rat cranial defect experiment, an 8-mm cranial defect was created by dentist's micro-drill after anesthetization as previously reported [36]. Once the scaffold was well placed into the defect, the skin incision was stitched up immedi-ately, followed by an intramuscular penicillin injection (20000 UI per rat). The animals were sacrificed at 4 and 12 weeks postoperatively. Residual scaffold and surrounding bone were harvested. In order to quantify the scaffold degradation and new bone formation, Micro-CT (SkyScan 1176, Broker, Germany) was used to get 3D reconstruction images. Considering that both the scaffold and bone were radiopaque, H&E and Masson's trichrome staining techniques were also applied for a comprehensive assessment of bone regeneration through comparing the mineralized and fibrous tissue growth within the three-dimensional scaffold.

2.7. Statistical analysis

All data were expressed as mean ± standard deviation and analyzed with SPSS software. One-way ANOVA was used for variance analysis between groups, and the level of significance was set at $p < 0.05$.

3. Results and discussion

3.1. Characterization of Zn/Sr doped hydroxyapatite co-assembled by collagen template

Collagen was the major organic component of the bone tissue, which could initiate and orientate the growth of bone apatite [37,38]. In this study, Zn/Sr co-substituted hydroxyapatite was self-assembled with the collagen template. The XRD results in Fig. 2A showed that four materials had a similar diffraction peaks distribution, and the main peaks were located near 26° and 32°, which were highly consistent with standard PDF card 09–0432 of hydroxyapatite. The FTIR spectra also presented typical hydroxyapatite-like vibration profiles. In Fig. 2B, vibration peaks appeared near 1034 cm^{-1}, 962 cm^{-1}, 603 cm^{-1}, 562 cm^{-1} and 471 cm^{-1}, which are the main characteristic peaks of PO_4^{3-} [39]. The bands centered at 1653 cm^{-1} and 1550 cm^{-1} represented amide I and amide II of collagen [11,40,41]. In addition, the bands at 1456 cm^{-1} and 874 cm^{-1} were attributed to CO_3^{2-} of B-type substituted hydroxyapatite, where the carbonate ion substitute appeared at the phosphate tetrahe-dron. The presence of CO_3^{2-} in the products was also proved by bands near 1339 cm^{-1}. The broad band at 3440 cm^{-1} was due to OH^{-1} or absorbed H_2O [39,42].

To further verify that the products were ion-doped, XRF was applied to quantify the element content in the powders, including element species and their molar ratio (Fig. 2C and Table 1). Fig. 2C confirmed that Zn and Sr were individually or co-doped into hydroxyapatite as designed. As shown in Table 1, all four kinds of products were Ca-deficient hydroxyapatite, whose Ca/P mole ratio was lower than 1.67 [43,44]. Using a multi-peak separation program with MDI Jade 6.0, the

Table 1
Molar ratio of different elements in hydroxyapatite.

Sample	M^{2+}/P	Zn/M^{2+}(%)	Sr/M^{2+}(%)
Col-HA	1.35		
Zn-Col-HA	1.57	3.76	
Sr-Col-HA	1.44		1.45
ZnSr-Col-HA	1.66	4.25	2.01

crystallinity of Col-HA, Zn-Col-HA, Sr-Col-HA, and ZnSr-Col-HA were determined as 32.75%, 27.42%, 44.14%, 51.89%, separately. Previous studies have illustrated that zinc ion is a potent inhibitor on hydroxy-apatite crystal growth, while Sr plays a positive role in the increase of hydroxyapatite crystallinity [45,46]. The organics adsorbed on hy-droxyapatite also have impacts on crystallinity as the more organics existed, the lower the crystallinity will be [47,48]. From the TG results (Fig. 2D and Table S3), it can be easily figured out that the collagen contents, which was the mass loss during 100–600 °C, were 20.5%, 16.1%, 18.8%, and 17.6% for Col-HA, Zn-Col-HA, Sr-Col-HA, and ZnSr-Col-HA, respectively. The lowest crystallinity of Zn-Col-HA and highest crystallinity of ZnSr-Col-HA might result from the combined effects of the species, contents of doped ions, and organic contents in products. Since the thermal stability was positively correlated with the crystallinity of materials, it was not surprising that Zn-Col-HA had the lowest phase transition temperature, reflected as the earliest endo-thermic peak appearance centered at 800 °C in the DSC curve (Sup-porting information Fig. S1).

The low crystallinity of the ion-doped hydroxyapatite co-assembled with collagen template allowed for a continuous ion release profile, shown in Fig. 2E. Considering the high concentration of Ca^{2+} in DMEM, Zn^{2+}/Sr^{2+} were very likely released as a substituted way by Ca^{2+}. The higher Ca-deficient level of Sr-Col-HA might be the main reason for a faster Sr^{2+} dissolution rate than ZnSr-Col-HA. While with a comparative M^{2+}/P molar ratio, the faster release rate of Zn^{2+} might attribute to the higher Zn^{2+} doped amount in ZnSr-Col-HA. Subsequently, the morphology of ion-doped hydroxyapatite was observed with SEM (Fig. 2F). Although ion substitution had an impact on hydroxyapatite morphology [16,49,50], there was no significant difference between the morphology of four kinds of materials in this study as they shared a short rod-like shape (Fig. 2F). It was speculated that the applied vast collagen template was the main contributing factor for the uniform morphology distribution, as reported previously [11,37]. The HRTEM results (Fig. 2G) with the crystalline and amorphous regions also verified that four products were low crystalline hydroxyapatite. These crystal planes observed in HRTEM were assigned to (002), (300), (112), (211), (210), and (102) lattice planes of hexagonal hydroxyapatite, which aligned with the XRD data.

3.2. The viability of RAW/BMSCs and osteo-immune response of macrophage co-cultured with ion-doped hydroxyapatite

As shown in Fig. 3A and B, all four materials had shown no cyto-toxicity to BMSCs and macrophages. Compared with the Col-HA group, Zn-Col-HA, Sr-Col-HA, and ZnSr-Col-HA groups showed better BMSCs and RAW viability, indicating a promoting effect of released Zn^{2+}/Sr^{2+} on cell proliferation. The highest cell viability of BMSCs co-cultured with RAW was found in ZnSr-Col-HA group, which further proved the best cytocompatibility of ZnSr-Col-HA (Fig. S2). We then evaluated the osteoimmunoregulatory effects of Zn/Sr doped hydroxyapatite by culturing macrophages with extracts of materials. Both the flow cytometry results of RAW and primary macrophages proved that ZnSr-Col-HA was most effective in activating the macrophages to M1 macrophage phenotype, followed by Zn-Col-HA, Sr-Col-HA and Col-HA, which indicated Zn^{2+} played a major role in this process (Fig. 3D, F and Fig. S3). The RT-PCR results further proved that, compared with the Col-HA group, the ion-doped hydroxyapatite extracts obviously activated the M1 macrophage phenotype with significant up-regulation of the expression of M1 macrophage markers CD11c and CCR7. (Fig. 3E and Fig. S4A). Typical pro-inflammatory cytokines, such as IL1β, IL6, and TNFα, displayed the highest expression in ZnSr-Col-HA, followed with Zn-Col-HA and Sr-Col-HA, while the lowest expression was found in Col-HA. Although Zn was usually regarded as an anti-inflammatory factor in serum level, by careful comparison between groups (Fig. 3C and F), we proposed that Zn might play a key role in high-level pro-inflammatory expression. Zn could induce increased pro-inflammatory expression in a
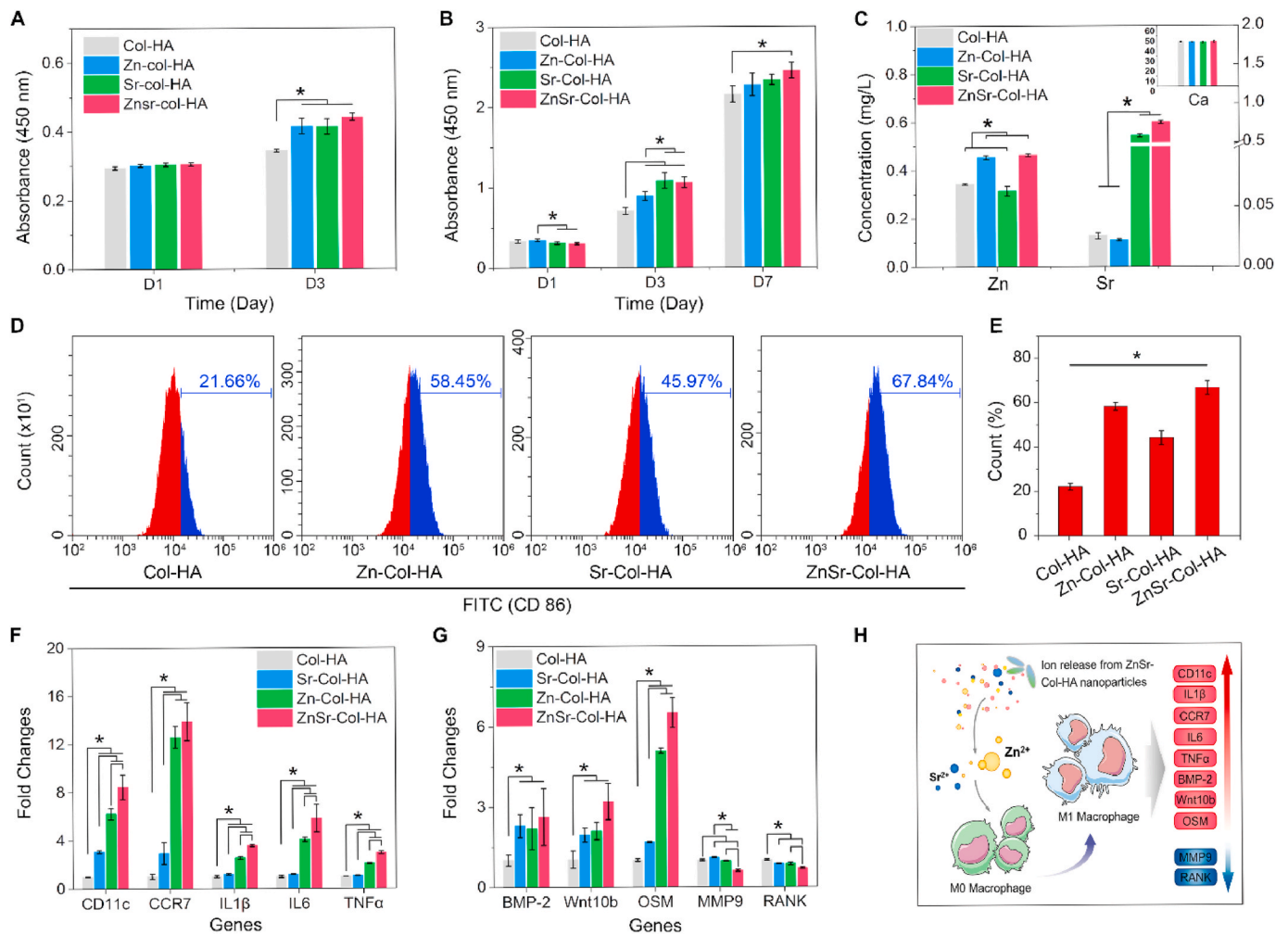
Fig. 3. The cytocompatibility and osteoimmunoregulatory ability of ZnSr-Col-HA. Cell viability of (A) RAW and (B) BMSCs cultured with different extractions. (C) Ion concentrations of conditioned medium determined by ICP-OES. (D) FACS results of RAW cells stimulated by different hydroxyapatite extractions for 24 h. (E) Quantitative results of FACS, n = 3, * indicated a significant difference p < 0.05. (F) Expression of M1 macrophages phenotypes genes (CD11c, CCR7) and pro-inflammatory cytokines (IL1β, IL6, TNFα) are significantly upregulated in Zn-Col-HA and ZnSr-Col-HA groups. (G) Expression of osteogenic genes (BMP-2, Wnt10b, OSM) and osteoclastic genes (MMP9, RANK) are remarkably upregulated and downregulated by Zn/Sr-doped hydroxyapatites, respectively. * indicated a significant difference p < 0.05, the cell used in (F) and (G) was RAW264.7. (H) Schematic of osteo-immune response of macrophages cultured with hydroxyapatite extractions.

dose-dependent way [51,52].

To explore the possible effects of four materials on osteogenesis, we also examined the expression level of some osteoclastogenic (MMP9, RANK) and osteogenic (BMP-2, Wnt10b, OSM) genes of RAW and primary macrophages, respectively (Fig. 3G and Fig. S4B). Both Zn^{2+} and Sr^{2+} could stimulate expression of BMP-2 and Wnt10b, while Zn^{2+} has a more obvious promotive effect on OSM expression, indicating Zn^{2+} was the primary regulated factor in the osteo-immune response of macrophages. As essential factors in osteogenesis, Zn^{2+} and Sr^{2+} showed a synergistic promoting effect on osteogenic gene expression, which were represented by the high expression level of osteogenic genes (BMP-2, Wnt10b, OSM) in ZnSr-Col-HA, especially OSM. The lowest gene expression of MMP9 and RANK in ZnSr-Col-HA further proved the critical role of Zn^{2+}. In contrast, high dose Sr^{2+} could be the primary cause of top-level MMP9 expression in Sr-Col-HA. The lowest expression levels of RANK in ZnSr-Col-HA also implied the combined effects of Zn^{2+} and Sr^{2+} on suppressing osteoclastogenesis. From the above results, we could figure out that the ZnSr-Col-HA extraction induced an active osteo-immune microenvironment containing abundant pro-inflammatory and osteogenic factors by stimulating macrophages (Fig. 3H), which could benefit bone regeneration.

3.3. The osteogenic differentiation of BMSCs under stimulation of conditioned medium

Osteoimmunology has revealed that host immune response and bone formation are closely related [1,53]. In this study, osteo-immune environment, modulated by macrophages/ion-doped hydroxyapatite extractions, was studied on its osteogenic effects. By culturing BMSCs with conditioned medium, we detected the expression levels of relevant osteogenic genes (Fig. 4). As an important marker for early osteogenic differentiation, ALP expression was qualitatively and quantificationally valuated. ZnSr-Col-HA showed the darkest dye color as well as the largest stained area (Fig. 4A). The similar tendency was also found in quantitative results, where ZnSr-Col-HA group presented a significantly higher ALP protein expression than other groups after a 3-day-culture with conditioned medium (Fig. 4B). Previous studies speculated that the osteo-immune microenvironment, including high expression of pro-inflammatory (IL1β, IL6, TNFα) and osteogenic cytokines (BMP2, Wnt10b, OSM), was beneficial for osteogenic differentiation of BMSCs [54,55]. We also verified that a favorable immune microenvironment was induced by macrophages treated with extractions of Zn/Sr-Col-HA, with a significantly enhanced osteogenic cytokine productions by
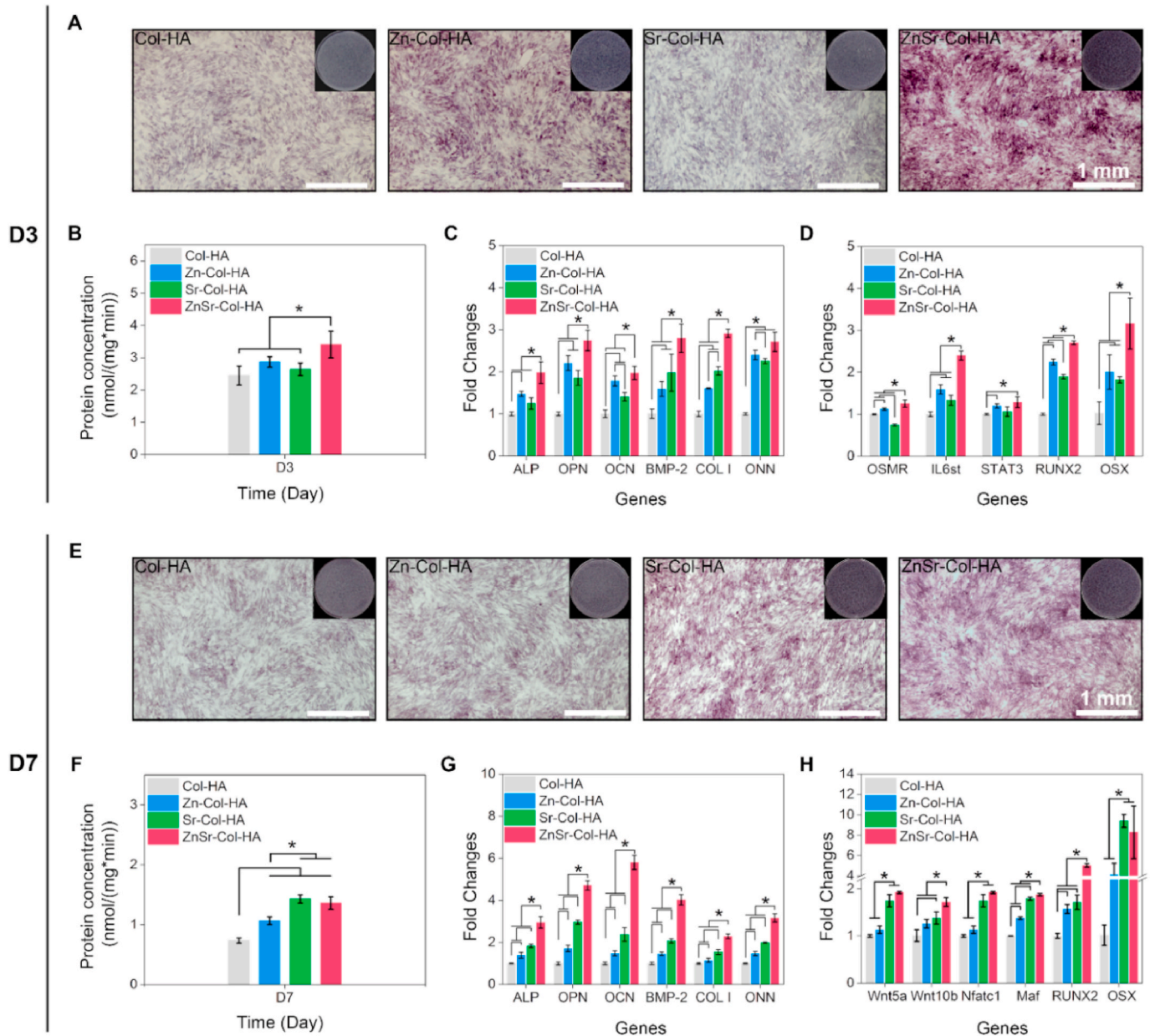
Fig. 4. Enhanced and procedural osteogenic factors expression of BMSCs by immune microenvironment stimulation. (A) ALP staining and (B) quantitative determination of ALP expression at D3. (C) Osteoblastic genes expression of BMSCs detected by RT-qPCR at D3. (D) Gene expression of OSM pathway mediators. (E) ALP staining and (F) quantitative determination of ALP expression at D7. (G) Osteoblastic genes expression of BMSCs detected by RT-qPCR at D7. (H) Gene expression of Nfatc1/Maf and Wnt pathway. * indicated a significant difference with $p < 0.05$.

BMSCs (Fig. 4C). By comparing the results (Fig. 3D and E and Fig. 4C), it was evident that not only the expression profile of osteogenic differentiation markers (ALP, COL I, OPN, OCN, ONN), but also the master regulators (BMP-2, OSX, RUNX2) secreted by BMSCs, were aligned with the expression tendency of the pro-inflammatory and osteogenic factors in osteo-immune microenvironment, which was modulated by macrophages/condition medium. Specifically, highest expression of osteogenic genes existed in ZnSr-Col-HA, followed by Zn-Col-HA and Sr-Col-HA, compared with Col-HA. Thus, we proposed that the osteo-immune microenvironment here was the primary cause for elevated BMSCs osteogenic factors expression at the early stage (D3).

We further explored the cell signaling pathway of osteogenesis, finding that the essential genes in the OSM pathway (OMSR/IL6st/STAT3) (Fig. 4D) were remarkably upregulated and had a similar tendency with pro-inflammatory factors (Fig. 3F), osteogenic factors

(Fig. 3G) and osteoblast differentiation master genes (Fig. 4C and D) expression, indicated that OSM pathway played a positive role on osteogenic genes expression (including OSX and RUNX2) and BMSCs differentiation to osteoblast in inflammatory environment at D3. With an extended incubation time, a high-level expression of ALP also existed in ion-doped groups compared with the Col-HA group (Fig. 4E and F). However, its trend was different from the profile of pro-inflammatory and other osteogenic factors expressed in the corresponding conditioned medium, and ALP expression ranked as group ZnSr-Col-HA, Sr-Col-HA, Zn-Col-HA, and Col-HA from high to low at D7. The RT-qPCR results of osteogenic factors expression further confirmed the discrepancy (Fig. 4G). Therefore, the osteo-immune microenvironment created by macrophages/hydroxyapatite extractions might not be the primary cause of stimulating osteogenic factors excretion in BMSCs at D7. It is known that Zn^{2+} and Sr^{2+}, even at trace doses, were potent osteogenesis

factors [56,57]. The ion concentrations of Zn^{2+} and Sr^{2+} in corresponding the conditioned media (Fig. 3C) had demonstrated a high positive correlation with expression levels of osteogenesis-related factors in Fig. 4G. Likely, Zn^{2+}/Sr^{2+} in conditioned media, especially Sr^{2+}, played a vital role in the expression of osteogenic genes at a later period (D7) (Fig. 4G). Through two osteogenic signaling pathways, Nfatc1/Maf and Wnt (Fig. 4H), Sr^{2+} significantly promoted the osteogenic differentiation of BMSCs (Fig. 4G), where Zn^{2+} acted as a synergy role. So far, we delineated the procedural promoting effects of ZnSr-Col-HA, where the osteogenic factors expressed in osteo-immune microenvironment played a major role in the early stage (D3), ion stimulating of Zn/Sr acted more effectively at the later stage (D7). Thus, it could be concluded that it was a modified potent method to co-dope Zn/Sr into hydroxyapatite through a biomimetic co-assembly way with the collagen template, allowing for better osteoimmunomodulatory and osteogenic capacities.

3.4. The in vivo evaluation on osteogenic effect and immune microenvironment of ion-doped hydroxyapatite

According to the latest research progress, bone regeneration is closely related to immune microenvironment around implant biomaterials [58,59]. The SD rat subcutaneous implantation model was used to evaluate the immune microenvironment around the implant scaffolds (Fig. S5). The H&E staining results (Fig. S5, upper) showed that all four ion-doped hydroxyapatite-based scaffolds could recruit macrophages to accelerate the scaffold degradation process, while ZnSr-Col-HA and Zn-Col-HA group owned a faster scaffold degradation rate, compared with Sr-Col-HA and Col-HA. It was found in immunofluorescence results (Fig. S5, bottom) that ZnSr-Col-HA and Zn-Col-HA
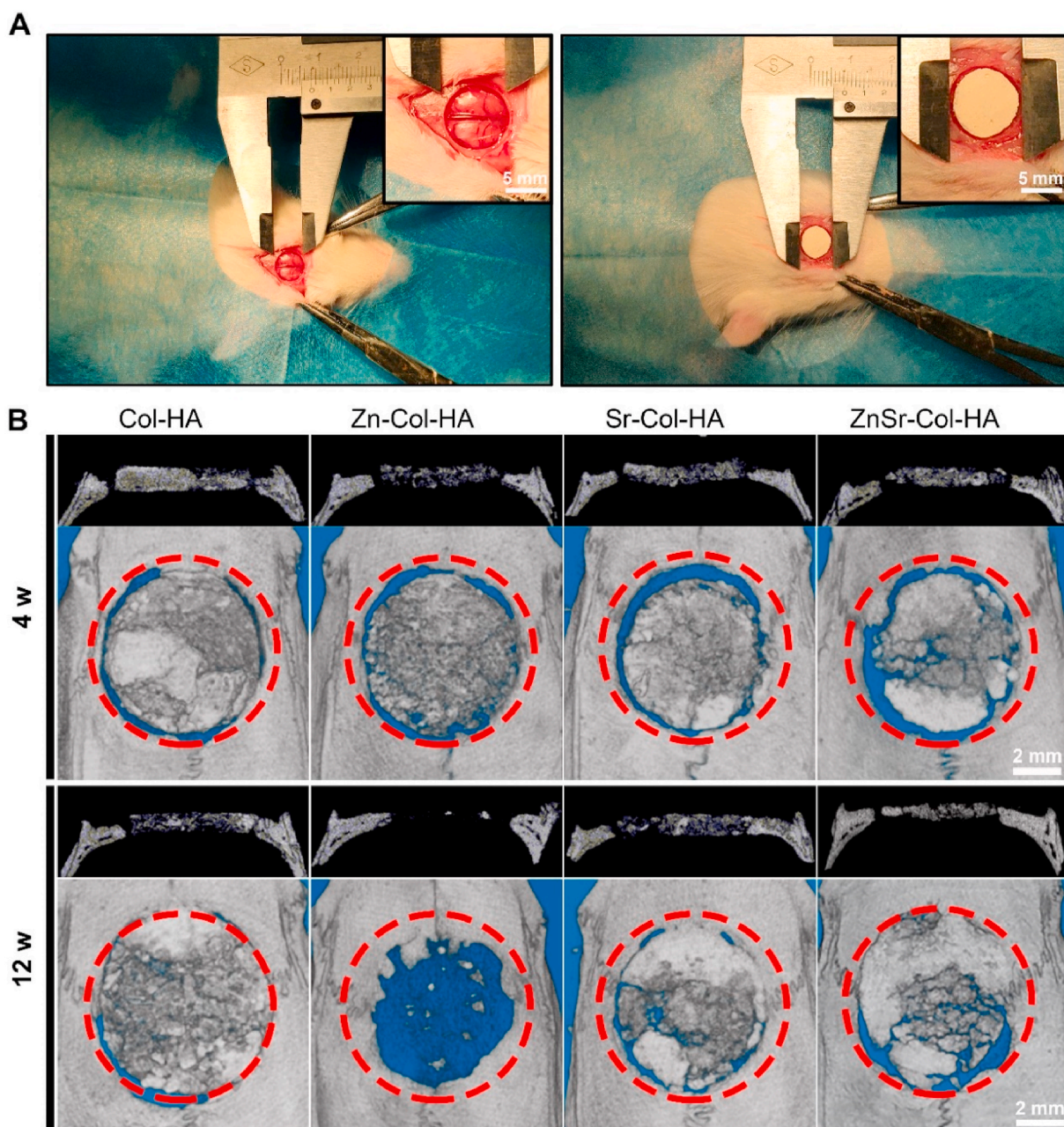
Fig. 5. Micro-CT analysis of rat cranial defect repair *in vivo*. (A) The surgery drawing of rat cranial defect and film repair. Rat cranial defects were treated with none (Blank), Col-HA, Zn-Col-HA, Sr-Col-HA and ZnSr-Col-HA scaffolds. (B) Micro-CT images of cranial defects showed different bone regeneration at 4 weeks and 12 weeks postoperatively. Upper, sectional view; bottom, 3D reconstruction images.

group activated more macrophages to M1 phenotype than Sr-Col-HA and Col-HA group, which was highly consistent with the *in vitro* results (Fig. 3D, E, F and Fig. S3, 4).

To assess the bone repair efficacy of ion-doped hydroxyapatite, we applied the SD rat critical-size cranial defect model for *in vivo* evaluation of different materials (Fig. 5A). Considering that the scaffolds with 70 wt

% inorganic minerals were radiopaque, both micro-CT and histological staining analysis were used to make a comprehensive assessment of bone regeneration. As shown in 3D reconstruction images (Fig. 5B), scaffold degradation and bone regeneration rates of four material groups were remarkably different from each other. Compared with the Col-HA scaffold, it can be easily found that the Zn-Col-HA scaffold has the fastest
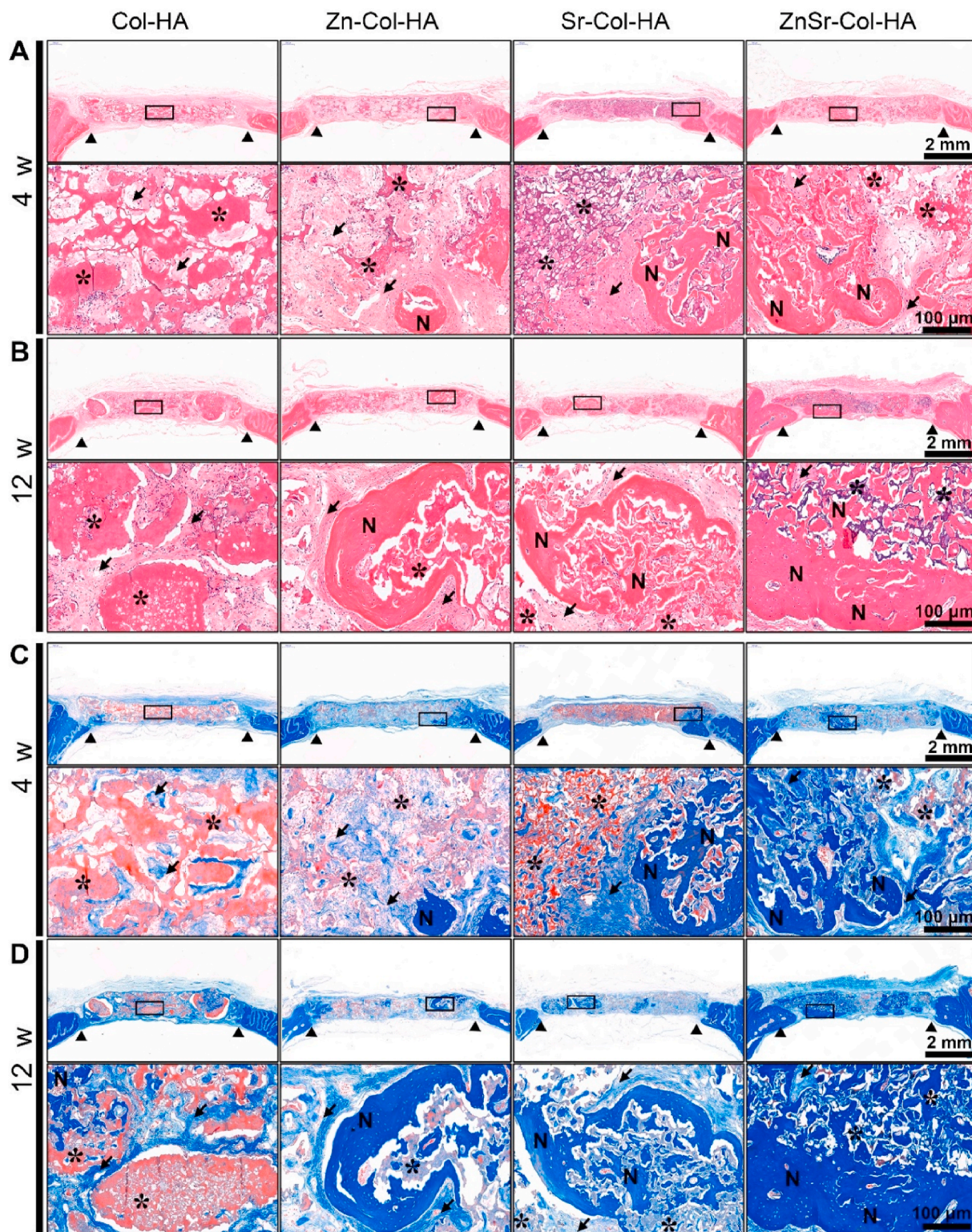
Fig. 6. H&E and Masson's trichrome staining analysis of cranial defects. Both H&E (A, B) and Masson's trichrome staining (C, D) results verified that ZnSr-Col-HA was able to significantly promote newly bone formation. Upper, overall view; bottom, zoom-in pictures of the rectangular box in the overall view. Black solid triangle, asterisk, arrow, and letter N indicated the border of cranial defects, scaffold, fibrous tissue, and new bone, respectively.

degradation rate, followed by ZnSr-Col-HA and Sr-Col-HA. Scaffold degradation *in vivo* is affected by the combined effects of various factors, including the local microenvironment and the physical/chemical properties of the scaffold itself. Considering the more distinct pro-inflammatory microenvironment in Zn-Col-HA/ZnSr-Col-HA group (Fig. 3D), it is easy to understand that ZnSr-Col-HA and Zn-Col-HA scaffold have a faster degradation rate than that of Sr-Col-HA and Col-HA scaffold (Fig. 5B). The degradation rate of the ZnSr-Col-HA scaffold is slower than that of the Zn-Col-HA scaffold, which may be due to the relatively higher crystallinity of ZnSr-Col-HA.

H&E staining results (Fig. 6A and B) revealed that new bone formation was visible in groups ZnSr-Col-HA, Sr-Col-HA and Zn-Col-HA. Furthermore, it could be easily figured out that the most abundant mature bone formation was in group ZnSr-Col-HA from Masson's trichrome staining (Fig. 6C and D), which represented ZnSr-Col-HA owned the most effective promoting capacity of bone regeneration. In contrast, the widest fibrous tissue distribution was observed in group Zn-Col-HA, which may be due to the mismatch between the rapid degradation of scaffold and slow bone formation. Both H&E and Masson's staining results showed that there was a most scaffold residues in group Col-HA at each time point. What's more, the largest amount of fibrous tissue and minimal bone formation were also existed in group Col-HA due to its relatively slow degradation rate compared to the other groups. The above results proved that Zn/Sr-hydroxyapatite co-assembled with collagen template was a promising biomaterial for bone repair due to its appropriate degradation rate and enhanced bone regeneration outcomes.

With the renascence of osteoimmunology, numerous studies had focused on the host immune response induced by bone biomaterials [53]. Hydroxyapatite, as a widely used orthopedic biomaterial, could regain attention in the bone repair field with the enhanced osteoimmunomodulatory capacity. Diverse material modification strategies, such as morphology manipulation and nano-structure design, could implement favorable osteoimmunomodulatory ability of hydroxyapatite [60,61]. Although ion substitution has been proved a potent way to reinforce the osteogenic capability of hydroxyapatite by activating cell behaviors related to skeletal system remodeling, few studies discussed its promoting effects on bone regeneration through regulating the immune system. This study, for the first time, explored the potential osteoimmunomodulatory effects of ion-doped hydroxyapatite. Two vital trace elements, Zn and Sr, were employed to synthesize Zn/Sr co-doped hydroxyapatite co-assembled with collagen template (ZnSr-Col-HA) through a biomimetic way. The physicochemical characterization confirmed Zn^{2+}/Sr^{2+} doping into hydroxyapatite and that ions could be released in DMEM in a sustained manner (Fig. 2).

Many studies have confirmed that osteogenesis is directly related to BMSCs *in vivo* [62,63]. Studies on bone immunology also suggested that macrophages play an important role in the process of osteogenesis *in vitro* [64,65] and *in vivo* [66,67]. Macrophage is an important cell type in immune system, which played the key role in the early period of inflammation and host defense in trauma repair after biomaterials implantation [3], It has been widely used as an model cell in the researches on modulating the immune response with biomaterials [68,69]. In this study, using macrophages as a simplified immune model cell, we found that ZnSr-Col-HA induced a favorable osteo-immune microenvironment for bone regeneration *in vitro* (Fig. 3), which was further confirmed by culturing BMSCs with conditioned medium produced by RAW treated with material extracts (Fig. 4). The potent osteogenic capacity of ZnSr-Col-HA was attested by repairing rat critical-size cranial defects *in vivo* (Figs. 5 and 6). These *in vitro* and *in vivo* studies indicated that the osteogenic effects of ZnSr-Col-HA could be divided into two stages (Fig. 1). At the first stage (before D3), an osteo-immune microenvironment induced by macrophages/ZnSr-Col-HA extraction promoted the expression of osteogenic genes in BMSCs. Specifically, Zn^{2+} played a major role in triggering the osteo-immune microenvironment. In the later stages (from D3 to D7), the residual Zn^{2+} and Sr^{2+} ions in conditioned medium were both responsible for promoting the expression of osteogenesis-related genes. The procedural promoting effects of ZnSr-Col-HA on BMSCs osteogenic gene expression indicated its potent osteoimmunomodulatory and osteogenic capacity. In addition, we found that ion co-substitution could greatly influence the degradation rate of hydroxyapatite by changing its crystallinity and surrounding immune microenvironment (Fig. 5B). As a result, appropriate choice of different ions conjunctively might be a solution to achieve a controlled degradation of hydroxyapatite.

Until now, to make hydroxyapatite more applicable in biomedicine, hydroxyapatite modification by ion doping was in a dilemma that hydroxyapatite biological performance might be more drastically affected by other material properties, such as grain size, morphology, and surface topology, rather than the dopant choice and concentration [70]. However, in our study, by combining Zn/Sr co-doping with molecular template assembly, ZnSr-Col-HA has shown favorable osteoimmunomodulatory and osteogenic capacity, it might be a potential solution for the predicament. This also inspires us that when designing biomaterials for bone defect repair, we should comprehensively consider the material's effects on the skeletal system and immune system to synergistically promote bone regeneration.

4. Conclusion

In summary, a rod-like Zn/Sr co-substituted hydroxyapatite (ZnSr-Col-HA) was successfully achieved by a biomimetic self-assembly method mediated by a collagen template. Zn^{2+} and Sr^{2+} could slowly and continuously release from ZnSr-Col-HA in DMEM and induce a proper osteo-immune microenvironment by stimulating macrophages, where expression of osteogenic genes (OSM, BMP-2, Wnt10b) were up-regulated and osteoclastogenesis-related factors (MMP-9, RANK) were down-regulated. Procedural promoting effects of ZnSr-Col-HA on osteogenesis-related gene expression by BMSCs were observed. The osteo-immune microenvironment induced by macrophages/ZnSr-Col-HA extraction and direct stimulating effects of Zn^{2+}/Sr^{2+} on BMSCs in conditioned medium acted as a pivotal role in different stages, respectively. Results of critical size rat cranial defect repair further confirmed the potent capacity of ZnSr-Col-HA in promoting bone regeneration *in vivo*. Therefore, ZnSr-Col-HA co-assembled through collagen template presents a type of potential biomaterials for orthopedic applications. The current strategy of combining ion doping and molecular assembly to endow hydroxyapatite bone immunomodulatory characteristics provides new inspiration and important prospect for the related studies on bone regeneration.

CRediT authorship contribution statement

Zhenyu Zhong: conceived the study and performed the experiments, data acquisition, and manuscript preparation. **Xiaodan Wu:** conceived the study and performed the experiments, data acquisition, and manuscript preparation. **Yifan Wang:** helped to analyze the data. **Mengdie Li:** assisted with materials characterization and cell experiments. **Yan Li:** assisted with materials characterization and cell experiments. **XuLong Liu:** assisted with materials characterization and cell experiments. **Xin Zhang:** assisted with materials characterization and cell experiments. **Ziyang Lan:** assisted with materials characterization and cell experiments. **Jianglin Wang:** helped in editing the manuscript. **Yingying Du:** Supervised the study and revised the manuscript. **Shengmin Zhang:** Supervised the study and revised the manuscript. All authors read and approved the final manuscript.

Declaration of competing interest

The authors declare no conflict of interest.

Appendix A. Supplementary data

Supplementary data to this article can be found online at https://doi.org/10.1016/j.bioactmat.2021.09.013.

References

[1] H. Takayanagi, Osteoimmunology: shared mechanisms and crosstalk between the immune and bone systems, Nat. Rev. Immunol. 7 (2007) 292–304.

[2] E. Gibon, L. Lu, S.B. Goodman, Aging, inflammation, stem cells, and bone healing, Stem Cell Res. Ther. 7 (2016) 44.

[3] S. Franz, S. Rammelt, D. Scharnweber, J.C. Simon, Immune responses to implants - a review of the implications for the design of immunomodulatory biomaterials, Biomaterials 32 (2011) 6692–6709.

[4] C. Wu, Z. Chen, Q. Wu, D. Yi, T. Friis, X. Zheng, et al., Clinoenstatite coatings have high bonding strength, bioactive ion release, and osteoimmunomodulatory effects that enhance in vivo osseointegration, Biomaterials 71 (2015) 35–47.

[5] Z. Chen, S. Ni, S. Han, R. Crawford, S. Lu, F. Wei, et al., Nanoporous microstructures mediate osteogenesis by modulating the osteo-immune response of macrophages, Nanoscale 9 (2017) 706–718.

[6] G. Liu, X. Wang, X. Zhou, L. Zhang, J. Mi, Z. Shan, et al., Modulating the cobalt dose range to manipulate multisystem cooperation in bone environment: a strategy to resolve the controversies about cobalt use for orthopedic applications, Theranostics 10 (2020) 1074–1089.

[7] S.L. Aktug, S. Durdu, E. Yalcin, K. Cavusoglu, M. Usta, Bioactivity and biocompatibility of hydroxyapatite-based bioceramic coatings on zirconium by plasma electrolytic oxidation, Mater. Sci. Eng. C Mater. Biol. Appl. 71 (2017) 1020–1027.

[8] R. Kiyama, T. Nonoyama, S. Wada, S. Semba, N. Kitamura, T. Nakajima, et al., Micro patterning of hydroxyapatite by soft lithography on hydrogels for selective osteoconduction, Acta Biomater. 81 (2018) 60–69.

[9] B. Ma, J. Han, S. Zhang, F. Liu, S. Wang, J. Duan, et al., Hydroxyapatite nanobelt/polylactic acid Janus membrane with osteoinduction/barrier dual functions for precise bone defect repair, Acta Biomater. 71 (2018) 108–117.

[10] O.R. Mahon, D.C. Browe, T. Gonzalez-Fernandez, P. Pitacco, I.T. Whelan, S. Von Euw, et al., Nano-particle mediated M2 macrophage polarization enhances bone formation and MSC osteogenesis in an IL-10 dependent manner, Biomaterials 239 (2020) 119833.

[11] G. Yang, H. Liu, X. Hu, Z. Chen, T.E. Friis, J. Wang, et al., Bio-inspired hybrid nanoparticles promote vascularized bone regeneration in a morphology-dependent manner, Nanoscale 9 (2017) 5794–5805.

[12] Y. Li, Y. Wang, N. Li, W. Luo, J. Jiang, J. Zhao, et al., Controllable synthesis of biomimetic hydroxyapatite nanorods with high osteogenic bioactivity, ACS Biomater. Sci. Eng. 6 (2019) 320–328.

[13] A. Shavandi, A.E.-D.A. Bekhit, Z.F. Sun, A. Ali, A review of synthesis methods, properties and use of hydroxyapatite as a substitute of bone, J. Biomimetics, Biomater. Biomed. Eng. 25 (2015) 98–117.

[14] H. Shi, X. Ye, J. Zhang, T. Wu, T. Yu, C. Zhou, et al., A thermostability perspective on enhancing physicochemical and cytological characteristics of octacalcium phosphate by doping iron and strontium, Bioact Mater. 6 (2021) 1267–1282.

[15] J. He, X. Hu, J. Cao, Y. Zhang, J. Xiao, L. Peng, et al., Chitosan-coated hydroxyapatite and drug-loaded polytrimethylene carbonate/polylactic acid scaffold for enhancing bone regeneration, Carbohydr. Polym. 253 (2021) 117198.

[16] J. Ma, J. Qin, Graphene-like zinc substituted hydroxyapatite, Cryst. Growth Des. 15 (2015) 7.

[17] S.C. Rui Zhao, Wanlu Zhao, Long Yang, Bo Yuan, Voicu Stefan Ioan, , Antoniac Vasile Iulian, Xiao Yang, Xiangdong Zhu, Xingdong Zhang, A bioceramic scaffold composed of strontium-doped three-dimensional hydroxyapatite whiskers for enhanced bone regeneration in osteoporotic defects, Theranostics 10 (2020) 1572–1589.

[18] W.L. Yu, T.W. Sun, Z.Y. Ding, C. Qi, H.K. Zhao, F. Chen, et al., Copper-doped mesoporous hydroxyapatite microspheres synthesized by a microwave-hydrothermal method using creatine phosphate as an organic phosphorus source: application in drug delivery and enhanced bone regeneration, J. Mater. Chem. B 5 (2017) 1039–1052.

[19] N.C. Andres, N.L. D'Elia, J.M. Ruso, A.E. Campelo, V.L. Massheimer, P.V. Messina, Manipulation of Mg(2+)-Ca(2+) switch on the development of bone mimetic hydroxyapatite, ACS Appl. Mater. Interfaces 9 (2017) 15698–15710.

[20] F.J. Martínez-Casado, M. Iafisco, J.M. Delgado-López, C. Martínez-Benito, C. Ruiz-Pérez, D. Colangelo, et al., Bioinspired citrate–apatite nanocrystals doped with divalent transition metal ions, Cryst. Growth Des. 16 (2016) 145–153.

[21] F.J. Martinez-Vazquez, M.V. Cabanas, J.L. Paris, D. Lozano, M. Vallet-Regi, Fabrication of novel Si-doped hydroxyapatite/gelatine scaffolds by rapid prototyping for drug delivery and bone regeneration, Acta Biomater. 15 (2015) 200–209.

[22] S. Kulanthaivel, U. Mishra, T. Agarwal, S. Giri, K. Pal, K. Pramanik, et al., Improving the osteogenic and angiogenic properties of synthetic hydroxyapatite by dual doping of bivalent cobalt and magnesium ion, Ceram. Int. 41 (2015) 11323–11333.

[23] F. Chen, P. Huang, Y.J. Zhu, J. Wu, C.L. Zhang, D.X. Cui, The photoluminescence, drug delivery and imaging properties of multifunctional Eu3+/Gd3+ dual-doped hydroxyapatite nanorods, Biomaterials 32 (2011) 9031–9039.

[24] S. Sprio, L. Preti, M. Montesi, S. Panseri, A. Adamiano, A. Vandini, et al., Surface phenomena enhancing the antibacterial and osteogenic ability of nanocrystalline hydroxyapatite, activated by multiple-ion doping, ACS Biomater. Sci. Eng. 5 (2019) 5947–5959.

[25] Z. Chen, J. Yuen, R. Crawford, J. Chang, C. Wu, Y. Xiao, The effect of osteoimmunomodulation on the osteogenic effects of cobalt incorporated beta-tricalcium phosphate, Biomaterials 61 (2015) 126–138.

[26] A. Szczes, L. Holysz, E. Chibowski, Synthesis of hydroxyapatite for biomedical applications, Adv. Colloid Interface Sci. 249 (2017) 321–330.

[27] M. Jia, Y. Hong, S. Duan, Y. Liu, B. Yuan, F. Jiang, The influence of transition metal ions on collagen mineralization, Mater. Sci. Eng. C Mater. Biol. Appl. 33 (2013) 2399–2406.

[28] S. Chen, Y. Shi, X. Zhang, J. Ma, Biomimetic synthesis of Mg-substituted hydroxyapatite nanocomposites and three-dimensional printing of composite scaffolds for bone regeneration, J. Biomed. Mater. Res. 107 (2019) 2512–2521.

[29] L. Yu, D.W. Rowe, I.P. Perera, J. Zhang, S.L. Suib, X. Xin, et al., Intrafibrillar mineralized collagen-hydroxyapatite-based scaffolds for bone regeneration, ACS Appl. Mater. Interfaces 12 (2020) 18235–18249.

[30] P. Bonaventura, G. Benedetti, F. Albarede, P. Miossec, Zinc and its role in immunity and inflammation, Autoimmun. Rev. 14 (2015) 277–285.

[31] A.S. Tiffany, D.L. Gray, T.J. Woods, K. Subedi, B.A.C. Harley, The inclusion of zinc into mineralized collagen scaffolds for craniofacial bone repair applications, Acta Biomater. 93 (2019) 86–96.

[32] S. Peng, X.S. Liu, G. Zhou, Z. Li, K.D. Luk, X.E. Guo, et al., Osteoprotegerin deficiency attenuates strontium-mediated inhibition of osteoclastogenesis and bone resorption, J. Bone Miner. Res. 26 (2011) 1272–1282.

[33] N. Rajan, J. Habermehl, M.F. Cote, C.J. Doillon, D. Mantovani, Preparation of ready-to-use, storable and reconstituted type I collagen from rat tail tendon for tissue engineering applications, Nat. Protoc. 1 (2006) 2753–2758.

[34] J. Wang, G. Yang, Y. Wang, Y. Du, H. Liu, Y. Zhu, et al., Chimeric protein template-induced shape control of bone mineral nanoparticles and its impact on mesenchymal stem cell fate, Biomacromolecules 16 (2015) 1987–1996.

[35] C. Hu, C. Chu, L. Liu, C. Wang, S. Jin, R. Yang, et al., Dissecting the microenvironment around biosynthetic scaffolds in murine skin wound healing, Sci. Adv. 7 (2021), eabf0787.

[36] B. Xu, P. Zheng, F. Gao, W. Wang, H. Zhang, X. Zhang, et al., A mineralized high strength and tough hydrogel for skull bone regeneration, Adv. Funct. Mater. 27 (2017) 1604327.

[37] Y. Wang, T. Azais, M. Robin, A. Vallee, C. Catania, P. Legriel, et al., The predominant role of collagen in the nucleation, growth, structure and orientation of bone apatite, Nat. Mater. 11 (2012) 724–733.

[38] J. Ma, J. Wang, X. Ai, S. Zhang, Biomimetic self-assembly of apatite hybrid materials: from a single molecular template to bi-/multi-molecular templates, Biotechnol. Adv. 32 (2014) 744–760.

[39] A. Antonakos, E. Liarokapis, T. Leventouri, Micro-Raman and FTIR studies of synthetic and natural apatites, Biomaterials 28 (2007) 3043–3054.

[40] C. Yanli, L. Chunyong, Z. Shengli, C. Zhenduo, X. Yang, Formation of bonelike apatite–collagen composite coating on the surface of NiTi shape memory alloy, Scripta Mater. 54 (2006) 89–92.

[41] M.C. Chang, J. Tanaka, FT-IR study for hydroxyapatite/collagen nanocomposite cross-linked by glutaraldehyde, Biomaterials 23 (2002) 4811–4818.

[42] L. Zou, Y. Zhang, X. Liu, J. Chen, Q. Zhang, Biomimetic mineralization on natural and synthetic polymers to prepare hybrid scaffolds for bone tissue engineering, Colloids Surf. B Biointerfaces 178 (2019) 222–229.

[43] O. Suzuki, S. Kamakura, T. Katagiri, M. Nakamura, B. Zhao, Y. Honda, et al., Bone formation enhanced by implanted octacalcium phosphate involving conversion into Ca-deficient hydroxyapatite, Biomaterials 27 (2006) 2671–2681.

[44] H. Guo, J. Su, J. Wei, H. Kong, C. Liu, Biocompatibility and osteogenicity of degradable Ca-deficient hydroxyapatite scaffolds from calcium phosphate cement for bone tissue engineering, Acta Biomater. 5 (2009) 268–278.

[45] M.D. O'Donnell, Y. Fredholm, A. de Rouffignac, R.G. Hill, Structural analysis of a series of strontium-substituted apatites, Acta Biomater. 4 (2008) 1455–1464.

[46] L. Wang, G.H. Nancollas, Calcium orthophosphates: crystallization and dissolution, Chem. Rev. 108 (2008) 4628–4669.

[47] T. Matsumoto, M. Okazaki, M. Inoue, Y. Hamada, M. Taira, J. Takahashi, Crystallinity and solubility characteristics of hydroxyapatite adsorbed amino acid, Biomaterials 23 (2002) 2241–2247.

[48] L. Wang, C. Li, Preparation and physicochemical properties of a novel hydroxyapatite/chitosan–silk fibroin composite, Carbohydr. Polym. 68 (2007) 740–745.

[49] H.B. Pan, Z.Y. Li, W.M. Lam, J.C. Wong, B.W. Darvell, K.D. Luk, et al., Solubility of strontium-substituted apatite by solid titration, Acta Biomater. 5 (2009) 1678–1685.

[50] Z. Zhong, J. Qin, J. Ma, Electrophoretic deposition of biomimetic zinc substituted hydroxyapatite coatings with chitosan and carbon nanotubes on titanium, Ceram. Int. 41 (2015) 8878–8884.

[51] Z. Chen, L. Chen, R. Liu, Y. Lin, S. Chen, S. Lu, et al., The osteoimmunomodulatory property of a barrier collagen membrane and its manipulation via coating nanometer-sized bioactive glass to improve guided bone regeneration, Biomater. Sci. 6 (2018) 1007–1019.

[52] P. Scuderi, Differential effects of copper and zinc on human peripheral blood monocyte cytokine secretion, Cell. Immunol. 126 (1990) 391–405.

[53] Z.T. Chen, T. Klein, R.Z. Murray, R. Crawford, J. Chang, C.T. Wu, et al., Osteoimmunomodulation for the development of advanced bone biomaterials, Mater. Today 19 (2016) 304–321.

[54] Y. Huang, C. Wu, X. Zhang, J. Chang, K. Dai, Regulation of immune response by bioactive ions released from silicate bioceramics for bone regeneration, Acta Biomater. 66 (2018) 81–92.

[55] M. Shi, L. Xia, Z. Chen, F. Lv, H. Zhu, F. Wei, et al., Europium-doped mesoporous silica nanosphere as an immune-modulating osteogenesis/angiogenesis agent, Biomaterials 144 (2017) 176–187.

[56] Y. Qiao, W. Zhang, P. Tian, F. Meng, H. Zhu, X. Jiang, et al., Stimulation of bone growth following zinc incorporation into biomaterials, Biomaterials 35 (2014) 6882–6897.

[57] M. Fenbo, X. Xingyu, T. Bin, Strontium chondroitin sulfate/silk fibroin blend membrane containing microporous structure modulates macrophage responses for guided bone regeneration, Carbohydr. Polym. 213 (2019) 266–275.

[58] C. Chu, J. Deng, L. Xiang, Y. Wu, X. Wei, Y. Qu, et al., Evaluation of epigallocatechin-3-gallate (EGCG) cross-linked collagen membranes and concerns on osteoblasts, Mater. Sci. Eng. C Mater. Biol. Appl. 67 (2016) 386–394.

[59] C. Chu, X. Zhao, S. Rung, W. Xiao, L. Liu, Y. Qu, et al., Application of biomaterials in periodontal tissue repair and reconstruction in the presence of inflammation under periodontitis through the foreign body response: recent progress and perspectives, J. Biomed. Mater. Res. B Appl. Biomater. (2021), https://doi.org/10.1002/jbm.b.34891. In press.

[60] L. Bai, Y. Liu, Z. Du, Z. Weng, W. Yao, X. Zhang, et al., Differential effect of hydroxyapatite nano-particle versus nano-rod decorated titanium micro-surface on osseointegration, Acta Biomater. 76 (2018) 344–358.

[61] C. Yang, C. Zhao, X. Wang, M. Shi, Y. Zhu, L. Jing, et al., Stimulation of osteogenesis and angiogenesis by micro/nano hierarchical hydroxyapatite via macrophage immunomodulation, Nanoscale 11 (2019) 17699–17708.

[62] Y. Liu, L. Ming, H. Luo, W. Liu, Y. Zhang, H. Liu, et al., Integration of a calcined bovine bone and BMSC-sheet 3D scaffold and the promotion of bone regeneration in large defects, Biomaterials 34 (2013) 9998–10006.

[63] J. Whitehead, K.H. Griffin, M. Gionet-Gonzales, C.E. Vorwald, S.E. Cinque, J. K. Leach, Hydrogel mechanics are a key driver of bone formation by mesenchymal stromal cell spheroids, Biomaterials 269 (2021) 120607.

[64] C. Chu, Y. Wang, Y. Wang, R. Yang, L. Liu, S. Rung, et al., Evaluation of epigallocatechin-3-gallate (EGCG) modified collagen in guided bone regeneration (GBR) surgery and modulation of macrophage phenotype, Mater. Sci. Eng. C Mater. Biol. Appl. 99 (2019) 73–82.

[65] C. Chu, J. Deng, Y. Man, Y. Qu, Evaluation of nanohydroxyapatite (nano-HA) coated epigallocatechin-3-gallate (EGCG) cross-linked collagen membranes, Mater. Sci. Eng. C Mater. Biol. Appl. 78 (2017) 258–264.

[66] W. Qiao, K.H.M. Wong, J. Shen, W. Wang, J. Wu, J. Li, et al., TRPM7 kinase-mediated immunomodulation in macrophage plays a central role in magnesium ion-induced bone regeneration, Nat. Commun. 12 (2021) 2885.

[67] P. Clezardin, R. Coleman, M. Puppo, P. Ottewell, E. Bonnelye, F. Paycha, et al., Bone metastasis: mechanisms, therapies, and biomarkers, Physiol. Rev. 101 (2021) 797–855.

[68] Z.T. Chen, S.W. Han, M.C. Shi, G.Q. Liu, Z.F. Chen, J. Chang, et al., Immunomodulatory effects of mesoporous silica nanoparticles on osteogenesis: from nanoimmunotoxicity to nanoimmunotherapy, Appl. Mater. Today 10 (2018) 184–193.

[69] Y. Zhu, Z. Ma, L. Kong, Y. He, H.F. Chan, H. Li, Modulation of macrophages by bioactive glass/sodium alginate hydrogel is crucial in skin regeneration enhancement, Biomaterials 256 (2020) 120216.

[70] V. Uskoković, Ion-doped hydroxyapatite: an impasse or the road to follow? Ceram. Int. 46 (2020) 11443–11465.